available at www.sciencedirect.com

ScienceDirect

journal homepage: www.elsevier.com/locate/biochempharm

Pharmacological characterization of recombinant N-type calcium channel ($Ca_v2.2$) mediated calcium mobilization using FLIPR

Elfrida R. Benjamin [*], *Farhana Pruthi* [2], *Shakira Olanrewaju* [2], *Shen Shan* [2], *Denise Hanway* [3], *Xuesong Liu* [4], *Rok Cerne* [5], *Daniel Lavery* [6], *Kenneth J. Valenzano* [1], *Richard M. Woodward* [7], *Victor I. Ilyin* [2]

Purdue Pharma Discovery Research, 6 Cedarbrook Drive, Cranbury, NJ 08512, United States

ARTICLE INFO

Article history:
Received 23 April 2006
Accepted 6 June 2006

Keywords:
N-type calcium channel
Calcium mobilization
Pharmacology
Sodium channel inhibitor
Antidepressant
Fluorescence imaging plate reader

Abbreviations:
Ctx-GVIa, ω-conotoxin GVIa
Ctx-MVIIa, ω-conotoxin MVIIa
EP, electrophysiology
FLIPR, fluorescence imaging plate reader
HEK-293, human embryonic kidney 293

ABSTRACT

The N-type voltage-gated calcium channel ($Ca_v2.2$) functions in neurons to regulate neurotransmitter release. It comprises a clinically relevant target for chronic pain. We have validated a calcium mobilization approach to assessing $Ca_v2.2$ pharmacology in two stable $Ca_v2.2$ cell lines: $\alpha1_B$, $\alpha2\delta$, β_3-HEK-293 and $\alpha1_B$, β_3-HEK-293. $Ca_v2.2$ channels were opened by addition of KCl and Ca^{2+} mobilization was measured by Fluo-4 fluorescence on a fluorescence imaging plate reader ($FLIPR^{96}$). $Ca_v2.2$ expression and biophysics were confirmed by patch-clamp electrophysiology (EP). Both cell lines responded to KCl with adequate signal-to-background. Signals from both cell lines were inhibited by ω-conotoxin (ctx)-MVIIa and ω-conotoxin (ctx)-GVIa with IC_{50} values of 1.8 and 1 nM, respectively, for the three-subunit stable, and 0.9 and 0.6 nM, respectively, for the two-subunit stable. Other known $Ca_v2.2$ blockers were characterized including cadmium, flunarizine, fluspirilene, and mibefradil. IC_{50} values correlated with literature EP-derived values. Novel $Ca_v2.2$ pharmacology was identified in classes of compounds with other primary pharmacological activities, including Na^+ channel inhibitors and antidepressants. Novel Na^+ channel compounds with high potency at $Ca_v2.2$ were identified in the phenoxyphenyl pyridine, phenoxyphenyl pyrazole, and other classes. The highest potency at $Ca_v2.2$ tricyclic antidepressant identified was desipramine.

© 2006 Elsevier Inc. All rights reserved.

[*] *Corresponding author at*: Amicus Therapeutics, Inc., 6 Cedar Brook Drive, Cranbury, NJ 08512, United States. Tel.: +1 609 662 2097; fax: +1 609 662 2002.
E-mail address: ebenjamin@amicustherapeutics.com (E.R. Benjamin).
[1] Present address: Amicus Therapeutics, 6 Cedar Brook Drive, Cranbury, NJ 08512, United States.
[2] Present address: Discovery Research, Purdue Pharma LP, 6 Cedar Brook Drive, Cranbury, NJ 08512, United States.
[3] Present address: Phenomix Corp., 5871 Oberlin Drive, Suite 200, San Diego, CA 92121, United States.
[4] Present address: Centocor Inc., 145 King of Prussia Road, Radnor, PA 19355, United States.
[5] Present address: Linguagen Corp., 2005 Eastpark Boulevard, Cranbury, NJ 08512, United States.
[6] Present address: Chromocell Corp., 675 U.S. Highway One, North Brunswick, NJ 08902, United States.
[7] Present address: Adolor Corp., 700 Pennsylvania Drive, Exton, PA 19341, United States.

0006-2952/$ – see front matter © 2006 Elsevier Inc. All rights reserved.
doi:10.1016/j.bcp.2006.06.003

Ca_v1, L-type voltage-gated calcium channel
$Ca_v2.2$, N-type voltage-gated calcium channel
PBSC, 4-(4-fluorophenoxy) benzaldehyde semicarbazone

1. Introduction

N-type voltage-gated calcium channel ($Ca_v2.2$) is a member of the voltage-dependent calcium channel family that also includes L-type ($Ca_v1.1$–$Ca_v1.4$), P/Q-type ($Ca_v2.1$), R-type ($Ca_v2.3$), and T-type ($Ca_v3.1$–3.3) [1]. $Ca_v2.2$ is predominantly expressed presynaptically in neurons and functions to regulate neurotransmitter release [2–5]. It plays an important role in mechanisms of neuronal hyperexcitability that can lead to pathological conditions such as chronic pain and ischemic brain injury [6,7]. Clinically, an antagonist of $Ca_v2.2$ has demonstrated efficacy for the treatment of human chronic pain [8]. $Ca_v2.2$ also affects cardiovascular function via regulation of catecholamine release from sympathetic neurons [2,9].

Native $Ca_v2.2$ is a hetero-oligomeric channel consisting of a core pore-forming subunit, $\alpha1_B$, and at least two auxiliary subunits, β and α2δ [10]. Multiple functionally distinct splice variant isoforms have been described for the $\alpha1_B$ subunit [11–13]. The β and α2δ subunits each arise from four distinct genes that also are alternatively spliced with multiple isoforms identified [14]. The β subunit that associates predominantly with $Ca_v2.2$ is β_3 [14]. The predominant $Ca_v2.2$ α2δ subunit remains to be resolved. Expression of $\alpha1_B$ alone can produce functional channels in *Xenopus* oocytes that are appropriately blocked by $Ca_v2.2$ selective ω-conotoxins, but which exhibit abnormal biophysical characteristics [15]. The presence of the auxiliary subunits increases $Ca_v2.2$ current amplitude, affects α1 subunit membrane trafficking, and modulates activation and inactivation kinetics of the channel [14]. Pharmacologically, the presence of the α2δ subunit reduces ω-conotoxin affinity for recombinant $Ca_v2.2$ channels [16] and constitutes a specific binding site for the anticonvulsant drug gabapentin [17].

Pharmacology of inhibition of native and recombinant $Ca_v2.2$ channel physiology is well characterized for ω-conotoxins such as ctx-MVIIa and ctx-GVIa [18–20]. Extensive radioligand binding analyses of these peptide inhibitors at $Ca_v2.2$ have also been described [21,22]. Other types of blockers of $Ca_v2.2$, such as the heavy metal cadmium and small organic molecule inhibitors, have been identified and characterized using electrophysiology (EP) [23–27]. Such reports have offered exquisitely detailed mechanistic analysis of compound-channel interaction for each particular inhibitor under investigation. However, when assessed collectively, comparison of pharmacological parameters such as rank order of potency for various blockers is difficult, as the data has been collected from a variety of neuronal and recombinant preparations with varied EP methods.

Calcium mobilization has also been used as a functional measurement of pharmacological parameters to support structure–activity relationship studies for several novel chemical classes of $Ca_v2.2$ blockers [28–33]. In most cases however, few or no classical $Ca_v2.2$ inhibitors were profiled in parallel with the new molecules for comparative purposes. Two studies did include ctx-MVIIa as a reference inhibitor and in one case high potency that approaches literature EP values was demonstrated (6 nM) [32]; in the other study however potency was very low (500 nM) [33]. Thus, pharmacological comparison of novel molecules from these studies to historical reference antagonists of $Ca_v2.2$ is not readily feasible.

The aim of this study was to provide a more comprehensive characterization of the pharmacology of $Ca_v2.2$ inhibitors in two recombinant cell lines: $\alpha1_B$, α2δ, β_3-HEK-293 and $\alpha1_B$, β_3-HEK-293 using calcium mobilization. This approach was validated with respect to potency and rank order for multiple classical $Ca_v2.2$ reference inhibitors of various chemical classes. Interestingly, responses were inhibited by small molecules known to exhibit voltage-dependent, frequency-dependent, and/or use-dependent mechanism of block. Specifically the voltage/frequency-dependent blockers flunarizine, fluspirilene, mibefradil, and the open channel blocker cadmium all exhibited appropriate pharmacology. $Ca_v2.2$ pharmacology was further extended via profiling of small molecules with previously uncharacterized $Ca_v2.2$ activity arising from classes of compounds with other primary pharmacologies, namely sodium (Na^+) channel inhibitors and antidepressants [34–38]. A preliminary account of this work has been published previously in abstract form [39].

2. Materials and methods

2.1. Materials

Cell culture and molecular biology reagents were purchased from Invitrogen Corporation (Carlsbad, CA) unless otherwise noted. Compounds that are not commercially available were synthesized to >97% purity as referenced. All other chemicals and reagents were purchased from Sigma (St. Louis, MO) unless otherwise noted.

2.2. Cloning of $Ca_v2.2$ subunit open reading frame (ORF) cDNAs

Alpha1B ($\alpha1_B$), beta3 (β_3), alpha2delta (α2δ) cDNAs encoding subunits of the rat $Ca_v2.2$ channel [40–42] were cloned by PCR amplification. The 7.0 kb cDNA containing the entire $\alpha1_B$ (ORF)

was PCR amplified as two overlapping cDNA fragments: a 2.7 kb 5′ fragment and a 4.4 kb 3′ fragment. The 5′ fragment was amplified from rat brain cDNA using forward and reverse primers CAC CAT GGT CCG CTT CGG GGAC and CCG TTC AGT GGC CTC CTCC, respectively. The 3′ fragment was amplified from rat spinal cord cDNA using forward and reverse primers CTA GCA CCA GTG ATC CTG GTC TG and AGT GCG TTG TGA GCG CAG TA, respectively. The two fragments were joined by ligation at a common restriction site to create the entire 7.0 kb cDNA. This ORF encodes the protein isoform generated by alternative splicing termed ''+A ΔSFMG ΔET'', which lacks the alternatively spliced four amino acid sequence SFMG that predominates in rat brain [11], but is presently unclear as to its relative abundance in spinal cord. The entire cDNA was sequenced with redundant coverage on both strands. The cDNA was then inserted into the mammalian expression vector pcDNA6.2DEST (Invitrogen, Carlsbad, CA) by homologous recombination using the Gateway system (Invitrogen).

The 1.45 cDNA encoding the β_3 subunit was cloned by PCR amplification from rat brain cDNA using forward and reverse primers CAC CAT GTA TGA CGA CTC CTAC and GGT GGT CAG TAG CTG TCC TTA GG, respectively. The 3.3 kb cDNA encoding the $\alpha 2\delta$ subunit was cloned by PCR amplification from rat brain cDNA using forward and reverse primers CAC CAT GGC TGC TGG CTG CCT and AGA GGG TCA CCA TAG TAG TGT CTG, respectively. PCR products were subcloned and fully sequenced on both strands. Clones matching the reference sequence (β_3: NM_012828; $\alpha 2\delta$: M86621) and the gene's GenBank rat genomic DNA sequences were recombined into the mammalian expression vector pcDNA3.2DEST (β_3) or pcDNA3.1-Zeo ($\alpha 2\delta$), which had been modified to a vector compatible with the Gateway recombination system using the Gateway vector adaptor kit (Invitrogen). Proper recombination was confirmed by sequencing of recombinogenic regions. For β_3 expression vector, proper protein expression was confirmed by Western blot analysis of lysates of transfected HEK-293 cells using a rabbit polyclonal antiserum directed against the rat β_3 subunit (USA Biological).

2.3. Stable $Ca_v2.2$ cell line development

$Ca_v2.2$ expressing HEK-293 cells were created in two stages. First, the rat $\alpha 1_B$, and β_3 cDNA expression constructs (2.5 μg each) were co-transfected into HEK-293 cells by Lipofectamine Plus reagent (Invitrogen), as per manufacturer's instructions. Twenty-four hours later cells were split in limiting dilution into multiple 96-well poly-D-lysine (PDL) coated plates (Becton Dickinson, Franklin Lakes, NJ) in selection media containing 20 μg/mL blasticidin and 500 μg/mL geneticin, and incubated for 3 weeks at 37 °C, 5% CO_2, 95% humidity. Plates containing ≤1 clone per well were cultured until wells positive for single clones were confluent. Individual clones were then arrayed into columns of a destination PDL-precoated 96-well plate and partly split into 6-well plates for culture maintenance. Array plates were washed once with assay buffer (127 mM NaCl, 1 mM KCl, 2 mM $MgCl_2$, 700 μM NaH_2PO_4, 5 mM $CaCl_2$, 5 mM $NaHCO_3$, 8 mM HEPES, 10 mM glucose, pH 7.4) and cells loaded for 1 h with 0.1 mL of assay buffer containing Fluo-4-AM (3 μM final concentration, Molecular Probes, Eugene, OR). Then they were washed twice with 0.1 mL of assay buffer, and replaced with 0.1 mL of the same. Plates were transferred to a Fluorimetric Imaging Plate Reader (FLIPR^{96}, Molecular Devices, Inc., Sunnyvale, CA) for assay. The FLIPR^{96} measured basal Fluo-4 fluorescence for 315 s, then added 0.1 mL KCl agonist dissolved in assay buffer and measured fluorescence for another 45 s. The final KCl concentration was 90 mM. Data were collected over the entire time course and analyzed using Microsoft Excel. The clone with the greatest signal-to-noise, stability of response with passage number, and adhesion to PDL-precoated plates was expanded and characterized. It constituted the $\alpha 1_B$, β_3-HEK cell line in these studies and also was used for stage 2 cell line development. The chosen clone was routinely grown and subcultured in Dulbecco's Modified Eagle Medium, 10% fetal bovine serum (HyClone, Logan, UT), 100 U/mL penicillin, 100 μg/mL streptomycin, 20 μg/mL blasticidin and 500 μg/mL geneticin, and incubated at 37 °C, 5% CO_2, 95% humidity. Cell division doubling time was approximately 24–48 h, and responses were stable for at least 15 passages.

Stage 2 of $Ca_v2.2$ cell line development was carried out as follows. The rat $\alpha 2\delta$ cDNA expression construct (5 μg) was transfected into the stage 1 $\alpha 1_B$, β_3-HEK cell line by Lipofectamine Plus reagent. Twenty-four hours later cells were split in limiting dilution into multiple 96-well PDL-precoated plates in selection media containing 20 μg/mL blasticidin, 500 μg/mL geneticin, and 250 μg/mL zeocin and incubated for 3 weeks at 37 °C, 5% CO_2, 95% humidity. Plates containing ≤1 clone per well were cultured and handled according to the same steps and procedures described above for the creation of stage 1 cell line. The three clones with the greatest signal-to-noise, stability of response with passage number, and adhesion to PDL-precoated plates were expanded, characterized and tested by EP for the largest current size, $Ca_v2.2$ pharmacology, $Ca_v2.2$ characteristic current–voltage relationship and kinetics, as described below. The chosen clone was routinely grown and subcultured in Dulbecco's Modified Eagle Medium, 10% fetal bovine serum (HyClone, Logan, UT), 100 U/mL penicillin, 100 μg/mL streptomycin, 20 μg/mL blasticidin, 500 μg/mL geneticin, and 250 μg/mL zeocin, and incubated at 37 °C, 5% CO_2, 95% humidity. This clone constituted the $\alpha 1_B$, $\alpha 2\delta$, β_3-HEK cell line in these studies. Cell division doubling time was approximately 24–48 h, and responses were stable for at least 15 passages.

2.4. $Ca_v2.2$ electrophysiology

For EP recording, the cells expressing $\alpha 1_B$, β_3 and $\alpha 2\delta$ subunits were seeded on PDL-precoated 35-mm culture Petri dishes (Becton Dickinson) at a density of approximately 10^4 cells/dish, and kept in an incubator for up to 3 days for subsequent recordings. For recordings, the dishes were positioned on the stage of an inverted microscope (Nikon, Eclipse E600, Japan) and superfused with a bath solution comprised of 11 mM $BaCl_2$, 1.5 mM $MgCl_2$, 10 mM HEPES, 120 mM TEA chloride, and 10 mM glucose adjusted to pH 7.4 with KOH, and osmolality set at 305 mOsmol. In a separate set of experiments, external $BaCl_2$ was replaced by physiologically more relevant 2 mM $CaCl_2$ or 5 mM $CaCl_2$, and osmolality set at 305 mOsmol. Whole-cell voltage-clamp recordings were made using conventional patch-clamp techniques [43] at room temperature (22–24 °C). The patch-clamp pipettes were pulled from WPI,

thick-walled borosilicate glass (WPI, Sarasota, FL). Currents were recorded using an Axopatch 200A amplifier (Axon Instruments/Molecular Devices Corporation, Union City, CA) and were leak-subtracted (P/4), low-pass filtered (1 kHz, 4-pole Bessel), digitized (20–50 μs intervals), and stored using Digidata 1200 B interface and Pclamp8.0/Clampex software (Axon Instruments). The pipettes were back-filled with internal solution containing 110 mM CsCl, 3 mM $MgCl_2$, 3 mM EGTA, 40 mM HEPES, 4 mM Mg-ATP, 0.5 mM Na_2GTP, adjusted to pH 7.2 with CsOH. Osmolality was set at around 295 mOsmol. The syringe with the internal solution for back-filling pipettes was kept on wet ice to preserve ATP/GTP integrity. The pipette resistance ranged from 2 to 3 MΩ; series resistance in the whole-cell configuration was in the range of 3–10 MΩ and was cancelled by 75–80% by the built-in electronic circuitry.

Cells were held at −90 mV and 20 ms pulses to 0 mV were applied every 20 s to monitor saturation of the initial run-up of the current. At this time-point the conventional current–voltage relationship was measured by a series of 15–80 ms depolarizing pulses incrementing in 10 mV steps. The holding voltage was then reset to −130 or −110 mV when the integrity of the cell membrane permitted. At this voltage most channels tend to remain in the resting state. A conventional double-pulse protocol was run to acquire the steady-state inactivation

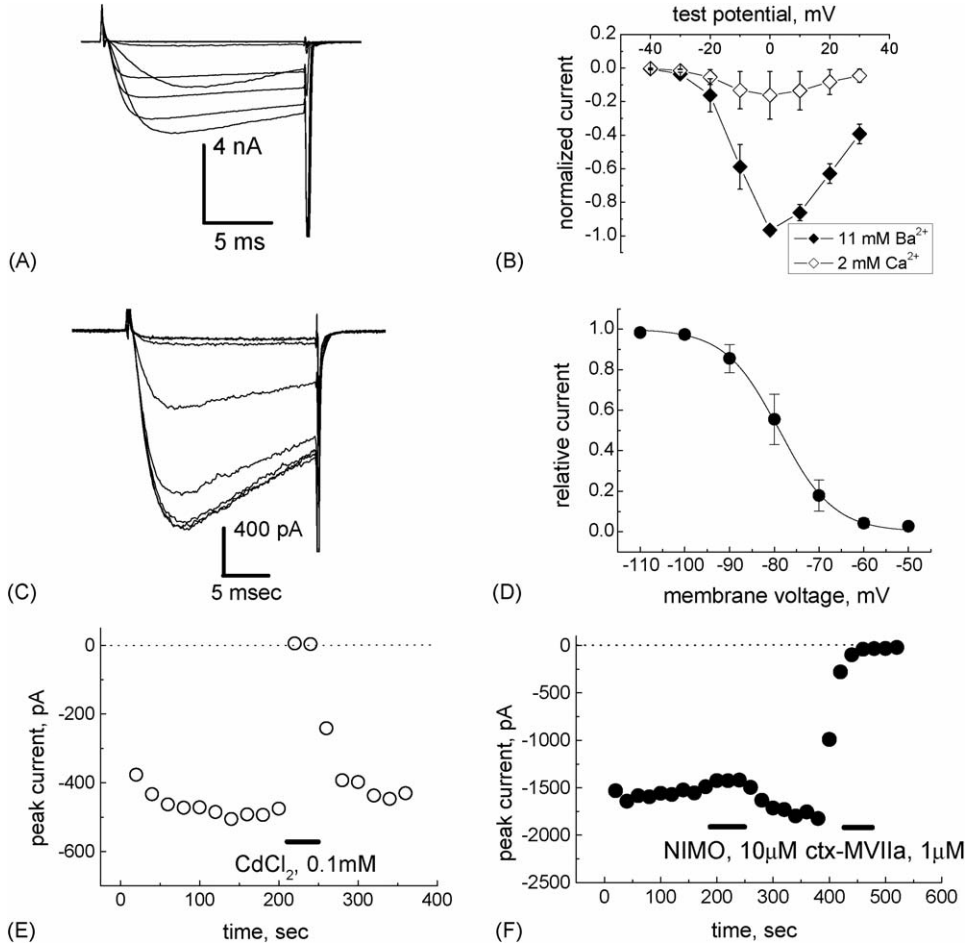

Fig. 1 – Activation, inactivation and pharmacological specificity of inward voltage-gated current in $\alpha 1_B$, $\alpha 2\delta$, β_3-HEK-293 cells. (A) Representative family of Ba^{2+} current traces caused by a series of depolarizing 15 ms long pulses from −40 to 30 mV with increments of 10 mV. Holding voltage was −100 mV. The tail currents at the end of depolarizing pulses were truncated. (B) Normalized current–voltage relationship averaged from five separate cells (filled diamonds). In four of these, additional current–voltage relationships were measured when 11 mM Ba^{2+} was replaced by 2 mM Ca^{2+}. Ca^{2+} currents (open diamonds), though smaller in size, were robust and showed similar voltage dependence. (C) Current traces in response to depolarizing pre-pulses incremented in 10 mV steps, applied for 3 s every 30 s then immediately followed by the 20 ms long test pulse to 0 mV. Holding voltage was −110 mV. (D) Peak current values in response to the test pulses were collected from six individual cells, averaged and plotted against corresponding pre-pulse voltages resulting in the mean steady-state inactivation curve fitted (solid line) with the Boltzmann function $1/(1 + \exp((V - V_{0.5})/k))$, where V is conditioning voltage, $V_{0.5}$ = −78.9 mV and k = 6 mV. (E) Rapid and fully reversible inhibition of inward current by 0.1 mM $CdCl_2$. Open circles correspond to the peak amplitude of currents in response to 20 ms long depolarizing pulses applied at 0.05 Hz. Data is representative of four such experiments with similar results. (F) Identical stimulation protocol as in panel E: weak and reversible inhibition of inward current by 10 μM nimodipine and fast, irreversible block by 1 μM ctx-MVIIa. Data is representative of four such experiments with similar results.

curve: 3 s long depolarizing pre-pulses incrementing in steps of 10 mV were immediately followed by a 20 ms long testing pulse to 0 mV to assess channel availability for activation. Subsequent episodes of stimulation were run at 0.033 Hz. To assess pharmacological specificity of the current, the holding voltage was reset back to −90 mV. Fractional inhibition of the currents by reference agents was measured using a 0.05 Hz train of 20 ms long depolarizing pulses to 0 mV.

Stock solutions of reference compounds were prepared in DMSO. Desired compound dilutions were prepared in bath solution, with a final DMSO concentration of 0.1%. The solutions were applied by gravity flow using a linear array of the glass pipes positioned about 200–300 μm apart from the cell and driven by a motor under remote control. This system permitted full solution exchange at the targeted cell within a few hundred milliseconds. All curve fitting of the patch-clamp data were carried out using Origin software (Version 5.0, Microcal). Data is presented as the mean ± S.E.M.

2.5. *Calcium mobilization assay for $Ca_v2.2$ using FLIPR^{96}*

One day prior to conducting this assay, $\alpha1_B$, $\alpha2\delta$, β_3- or $\alpha1_B$, β_3-HEK-293 cells were seeded onto PDL-precoated 96-well clear-bottom black plates at 75,000 cells/well. On the day of the assay, the cell plates were washed with assay buffer (127 mM NaCl, 1 mM KCl, 2 mM $MgCl_2$, 700 μM NaH_2PO_4, 5 mM $CaCl_2$, 5 mM $NaHCO_3$, 8 mM HEPES, 10 mM glucose, pH 7.4), then loaded and pretreated with compounds for 1 h as follows: 0.05 mL of each compound diluted at a 2× concentration in assay buffer containing 20 μM nifedipine plus 0.05 mL of assay buffer containing 6 μM Fluo-4-AM were added, for a final compound concentration of 1×, a final nifedipine concentration of 10 μM, and a final Fluo-4-AM concentration of 3 μM. The nifedipine was included to block any endogenous Ca_v1 response to KCl. Cells were incubated at 37 °C for 1 h, then washed once with 0.1 mL of compound diluted at a 2× concentration in 20 μM nifedipine containing assay buffer (no Fluo-4-AM). Cells were then replaced with 0.1 mL of each compound diluted at a 2× concentration in 20 μM nifedipine containing assay buffer. Plates were then transferred to a FLIPR^{96} for assay. The FLIPR^{96} measured basal Fluo-4 fluorescence for 5 min and 15 s (315 s), then added 0.1 mL KCl dissolved in assay buffer and measured fluorescence for another 45 s. Final test compound concentrations on the cells after FLIPR read ranged from about 508 pM to about 50 μM, final nifedipine concentration was 5 μM, and final KCl concentration was 90 mM. Final DMSO concentration was held constant at 0.5%. Data were collected over the entire time course of the FLIPR^{96} read.

The protocol for a 5 min compound pretreatment calcium mobilization assay was similar to that of the 1 h assay, but with the following changes. Cells were loaded with 0.1 mL of assay buffer containing 20 μM nifedipine and 6 μM Fluo-4-AM for 1 h at 37 °C. Cells were then washed once with 0.1 mL assay buffer containing 20 μM nifedipine, then replaced with 0.05 mL of the same. Plates were then transferred to the FLIPR^{96}. Basal Fluo-4 fluorescence was measured for 15 s, then 0.05 mL of each compound diluted at a 4× concentration in assay buffer was added, and fluorescence was read for another 5 min. Then 0.1 mL KCl dissolved in assay buffer was added and fluorescence measured for another 45 s. Final compound

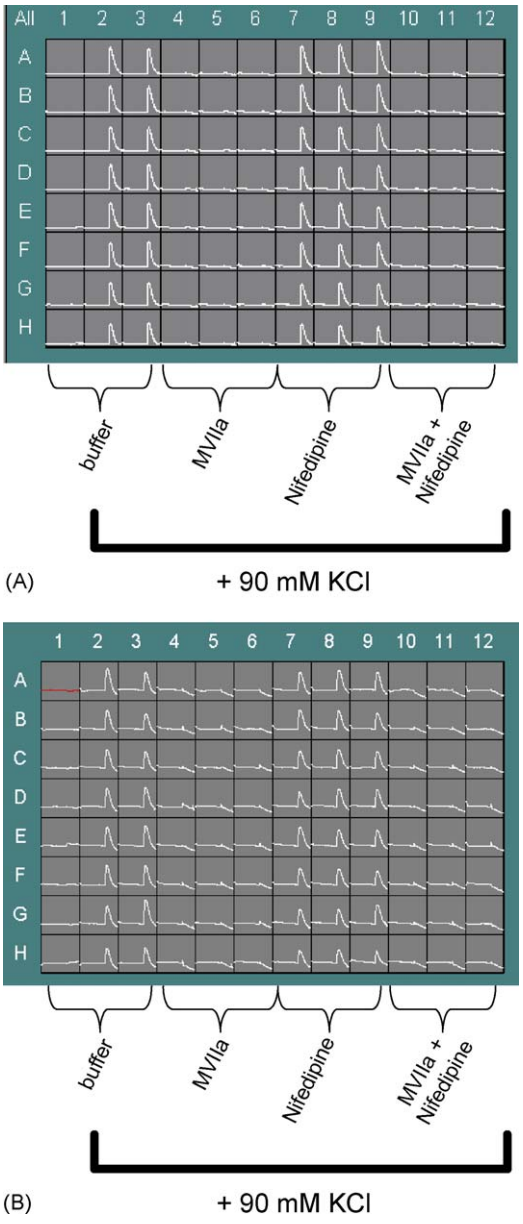

Fig. 2 – Calcium mobilization responses to KCl depolarization measured on FLIPR^{96} in $\alpha1_B$, $\alpha2\delta$, β_3-HEK-293 and $\alpha1_B$, β_3-HEK-293 cells. (A) A representative 96-well plate of $\alpha1_B$, $\alpha2\delta$, β_3-HEK-293 cell responses to 90 mM KCl in the presence or absence of inhibitors is illustrated. Column 1 is the negative control response to buffer addition. KCl (90 mM) was added to the rest of the columns after 5 min pretreatment with either buffer (columns 2–3), 250 nM ctx-MVIIa (columns 4–6), 10 μM nifedipine (columns 7–9), or the same concentrations of ctx-MVIIa and nifedipine combined (columns 10–12). This plate is representative of five with similar results. (B) A representative 96-well plate of $\alpha1_B$, β_3-HEK-293 cell responses to 90 mM KCl in the presence or absence of inhibitors is illustrated. The plate layout is the same as described in panel A. This plate is representative of three with similar results.

concentration ranges as well as nifedipine, KCl, and DMSO concentrations were the same as for the 1 h protocol. Data collection and analysis were also the same.

2.6. Data analysis

Experiments were expressed as percentage of control. This refers to the average of multiple determinations normalized to the maximum average counts in the presence of 90 mM KCl and to the minimum average counts in the presence of 50 nM ω-ctx GVIa block of 90 mM KCl. Normalization calculations were conducted using GraphPad Prism Version 3.02 software (San Diego, CA) or Microsoft Excel. Theoretical curves were generated using nonlinear regression curve-fitting analysis in GraphPad Prism Version 3.02. Linear regression analysis was carried out using GraphPad Prism Version 3.02.

3. Results

$Ca_v2.2$ currents were characterized by EP in the $\alpha1_B$, $\alpha2\delta$, β_3-HEK cell for biophysical properties and pharmacological specificity. At a holding potential of −90 mV, currents in response to 20 ms depolarizing pulses to 0 mV at 0.05 Hz were allowed to stabilize for approximately 3 min to avoid interference from initial current run-up observed shortly after attaining whole cell configuration. In Ba^{2+} saline solution, currents of maximum magnitude of ≥0.5 nA were typically observed (Fig. 1A). Threshold of activation was approximately −40 to −30 mV, and current peaked at −10 to 0 mV (Fig. 1B). For the set of experiments, described in Fig. 1A and B, the mean maximum current was 3.3 ± 0.9 nA (n = 5). When external Ba^{2+} was replaced by 2 mM Ca^{2+}, the mean maximum current dropped to 0.75 ± 0.22 nA (n = 4). There was no shift in the current–voltage relationship. In the presence of 5 mM Ca^{2+}, the concentration used in the FLIPR assay buffer, the mean maximal current was approximately 50% of the current in the presence of 11 mM Ba^{2+}, without any shift in the current–voltage relationship (data not shown). Steady-state inactivation curves were obtained after 3 s pre-pulse depolarization conducted in 10 mV increments between −110 and −50 mV (Fig. 1C and D). The peak current to the test pulse was plotted versus the amplitude of depolarizing pre-pulse and the Boltzmann equation was fit to the data allowing an estimate of half-inactivation voltage, $V_{0.5}$, and a slope factor, k. As measured in six separate cells, the mean values were $V_{0.5} = -79.2 \pm 2.4$ mV and $k = 4.6 \pm 0.2$ mV. The steady-state inactivation curve shifted to the left at longer depolarizing pre-pulses and more negative holding voltages (data not shown). To characterize the pharmacological specificity of the current, $Ca_v2.2$ inhibitors cadmium and ctx-MVIIa were used as $Ca_v2.2$ positive controls, and nimodipine, a Ca_v1 inhibitor, was used

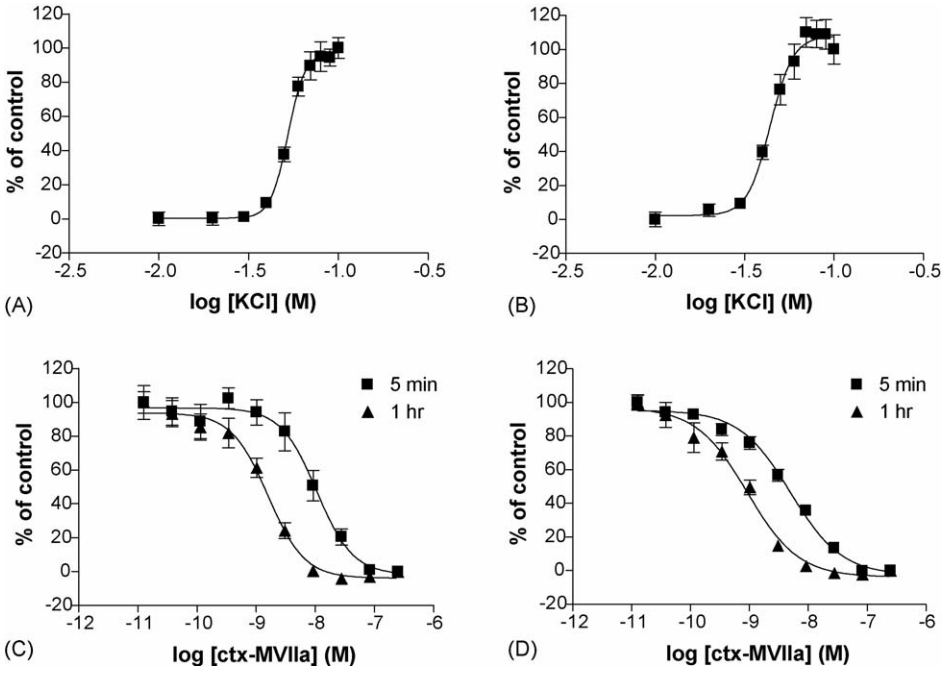

Fig. 3 – Concentration-dependent KCl stimulation and ctx-MVIIa inhibition of calcium responses measured on FLIPR^{96} in $\alpha1_B$, $\alpha2\delta$, β_3- and $\alpha1_B$, β_3-HEK-293 cells. (A) Concentration-dependent stimulation of the calcium mobilization response to KCl in $\alpha1_B$, $\alpha2\delta$, β_3-HEK-293 cells. Data points are the mean ± S.E.M. of eight wells from one plate representative of four. (B) Concentration-dependent stimulation of the calcium mobilization response to KCl in $\alpha1_B$, β_3-HEK-293 cells. Data points are the mean ± S.E.M. of eight wells from one plate representative of three. (C) Five minutes and 1 h ctx-MVIIa pretreatment mediated concentration-dependent inhibition of the calcium mobilization response to 90 mM KCl in $\alpha1_B$, $\alpha2\delta$, β_3-HEK-293 cells. Data points are the mean ± S.E.M. of eight wells from one plate representative of three (5 min) or five (1 h). (D) Five minutes and 1 h ctx-MVIIa pretreatment mediated concentration-dependent inhibition of the calcium mobilization response to 90 mM KCl in $\alpha1_B$, β_3-HEK-293 cells. Data points are the mean ± S.E.M. of eight wells from one plate representative of three (5 min) or four (1 h).

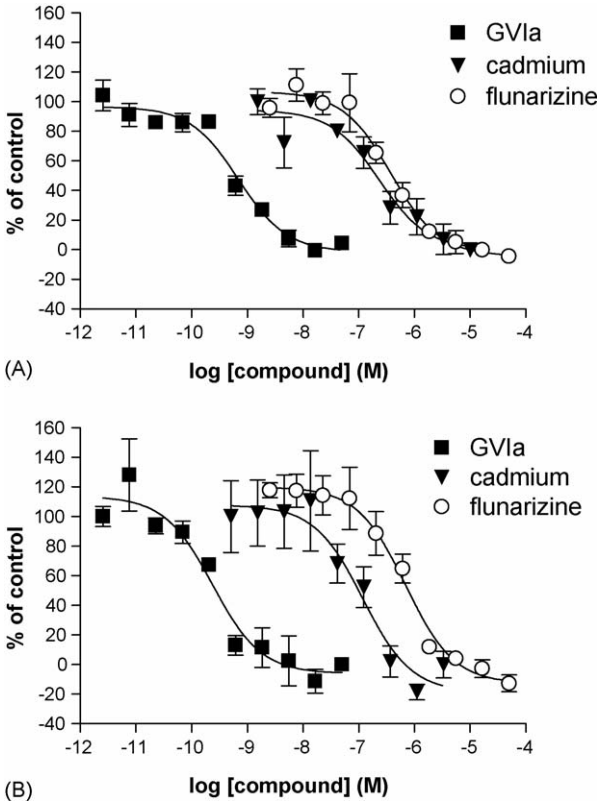

Fig. 4 – Concentration-dependent $Ca_v2.2$ reference antagonist inhibition of calcium responses measured on FLIPR^{96} in $\alpha1_B$, $\alpha2\delta$, β_3- and $\alpha1_B$, β_3-HEK-293 cells. (A) ctx-GVIa-, cadmium-, and flunarizine-mediated concentration-dependent inhibition of the calcium mobilization response to 90 mM KCl in $\alpha1_B$, $\alpha2\delta$, β_3-HEK-293 cells. Data points are the mean ± S.E.M. of four wells from one plate representative of 4–6. (B) Same compounds as panel A measured from $\alpha1_B$, β_3-HEK-293 cells. Data points are the mean ± S.E.M. of four wells from one plate representative of 3–7.

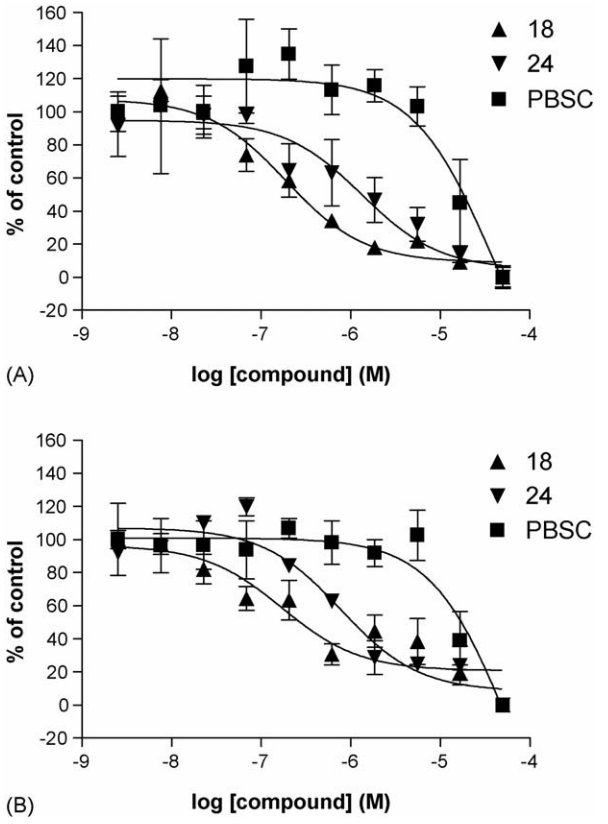

Fig. 5 – Concentration-dependent reference Na^+ channel antagonist inhibition of calcium responses measured on FLIPR^{96} in $\alpha1_B$, $\alpha2\delta$, β_3- and $\alpha1_B$, β_3-HEK-293 cells. (A) Compound 18 [52], compound 24 [51], and PBSC [51] mediated concentration-dependent inhibition of the calcium mobilization response to 90 mM KCl in $\alpha1_B$, $\alpha2\delta$, β_3-HEK-293 cells. Data points are the mean ± S.E.M. of four wells from one plate representative of 3–5. (B) Same compounds as panel A measured from $\alpha1_B$, β_3-HEK-293 cells. Data points are the mean ± S.E.M. of four wells from one plate representative of 3–6.

as a negative control (Fig. 1E and F). Cadmium (0.1 mM) block was fast, complete and reversible upon wash-out. ctx-MVIIa (1 μM) blocked with slower kinetics, but was complete within 3–6 min, and was irreversible. Nimodipine (10 μM) block was weak and reversible. Thus, current properties and pharmacology from the $\alpha1_B$, $\alpha2\delta$, β_3-HEK cells fundamentally resembled those of previously reported native and recombinant $Ca_v2.2$ [44,45]. In contrast, currents from $\alpha1_B$, β_3-HEK cells were small (≤200 pA), less reliable, and unfeasible for characterization of $Ca_v2.2$ biophysics or pharmacology (data

Table 1 – FLIPR IC_{50} vs. EP IC_{50} values of six reference $Ca_v2.2$ inhibitors

Compound	FLIPR IC_{50} (nM)		Literature EP	
	$\alpha1_B$, $\alpha2\delta$, β_3	$\alpha1_B$, β_3	IC_{50} (nM)	Reference
Ctx-GVIa	0.98 ± 0.2 (6)	0.6 ± 0.2 (7)	0.7	[19]
Ctx-MVIIa	1.8 ± 0.24 (5)	0.9 ± 0.1 (4)	1.0	[20]
Cadmium	288 ± 43 (4)	114 ± 4.1 (3)	655	[26]
Flunarizine	743 ± 148 (4)	560 ± 170 (4)	800	[27]
Fluspirilene	1359 ± 255 (3)	1297 ± 239 (3)	2000	[24]
Mibefradil	2394 ± 723 (3)	1746 ± 334 (3)	3100	[23]

Values represent mean ± S.E.M. (*n*). N-VGCC EP IC_{50} values are derived from the literature as referenced.

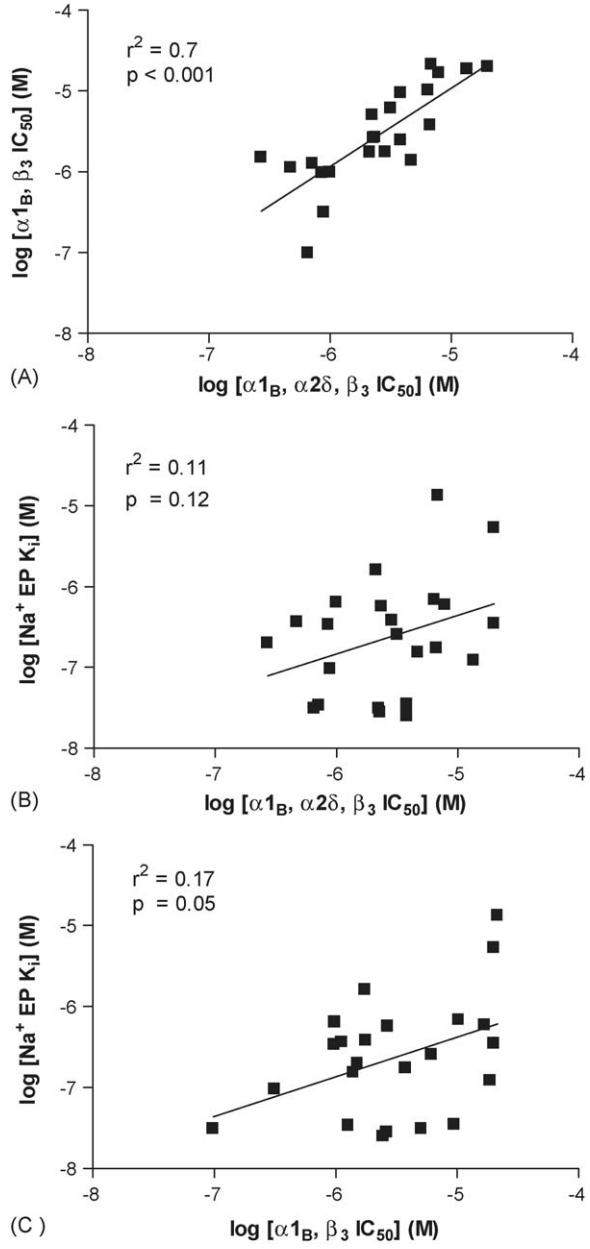

Fig. 6 – Correlation analysis of IC_{50} values for compound inhibition of calcium responses comparing the two $Ca_v2.2$ cell lines, or comparing each cell line and published Na^+ K_i values. (A) Correlation analysis between the $\alpha1_B$, $\alpha2\delta$, β_3- and $\alpha1_B$, β_3-HEK-293 cell IC_{50} values for $Ca_v2.2$ inhibition of the known Na^+ channel inhibitor compounds listed in Table 2. Significant correlation is observed for this set of 23 compounds of varying chemotypes. Data from the 16 compounds in Tables 1 and 3 are not included in this panel, for the sake of comparison to subsequent panels in this figure. However, the correlation with those additional 16 compounds included also is significant: $r^2 = 0.91$, $p < 0.0001$. (B) Correlation analysis between the $\alpha1_B$, $\alpha2\delta$, β_3-HEK-293 cell IC_{50} values and published Na^+ channel K_i values determined by EP. No significant correlation is observed. (C) Correlation analysis between the $\alpha1_B$, β_3-HEK-293 cell IC_{50} values and published Na^+ channel K_i values determined by EP. No significant correlation is observed.

not shown), consistent with the well characterized role of the $\alpha2\delta$ subunit in enhancement of calcium channel current amplitude [46].

Calcium responses to KCl (90 mM) were evaluated on a FLIPR^{96} in the $\alpha1_B$, $\alpha2\delta$, β_3-HEK (Fig. 2A) and $\alpha1_B$, β_3-HEK (Fig. 2B) cell lines. KCl elicited a reproducible response that was completely inhibited by 250 nM ctx-MVIIa. However nifedipine (10 μM), a selective Ca_v1 blocker, had no effect. Combined ctx-MVIIa plus nifedipine blocked the response similar to ctx-MVIIa alone. The average signal-to-background, as determined by fluorescence change (ΔF) after 90 mM KCl divided by ΔF after buffer alone was 24 ± 9 ($n = 5$ plates) and 18 ± 1 ($n = 3$ plates) in the $\alpha1_B$, $\alpha2\delta$, β_3-HEK and $\alpha1_B$, β_3-HEK cells, respectively. The KCl-induced calcium response was concentration-dependent (Fig. 3A and B). The average EC_{50} values were 55 ± 5 mM ($n = 4$) and 50 ± 7 mM ($n = 3$) in the $\alpha1_B$, $\alpha2\delta$, β_3-HEK and $\alpha1_B$, β_3-HEK cells, respectively. The effect of compound pretreatment time (5 min versus 1 h) on the concentration-dependence of ctx-MVIIa inhibition of the response to 90 mM KCl was also evaluated in $\alpha1_B$, $\alpha2\delta$, β_3-HEK and $\alpha1_B$, β_3-HEK cells (Fig. 3C and D). The 1 h pretreatment protocol yielded higher potency of ctx-MVIIa in both cell lines. In $\alpha1_B$, $\alpha2\delta$, β_3-HEK cells, the average IC_{50} for the 5 min and 1 h protocol was 21 ± 7 nM ($n = 3$) and 1.8 ± 0.24 nM ($n = 5$), respectively. In $\alpha1_B$, β_3-HEK cells, the average IC_{50} for the 5 min and 1 h protocol was 6 ± 2 nM ($n = 3$) and 0.9 ± 0.1 nM ($n = 4$), respectively. The 1 h IC_{50} values more closely match the reported EP literature value (1 nM) [26], and thus this protocol was used for all pharmacological characterization of $Ca_v2.2$ in these cells.

The pharmacology of classical $Ca_v2.2$ reference inhibitors of varying chemical classes was characterized in the $\alpha1_B$, $\alpha2\delta$, β_3-HEK and $\alpha1_B$, β_3-HEK cells. Similar to ctx-MVIIa, ctx-GVIa, a selective peptide inhibitor of $Ca_v2.2$, potently inhibited the calcium response to 90 mM KCl in both cell lines (Fig. 4, Table 1). Cadmium, a heavy metal pore blocker, exhibited intermediate potency (Fig. 4, Table 1). Small organic $Ca_v2.2$ inhibitor compounds of diverse chemical classes such as flunarizine, a piperazine, flusiprilene, a diphenylbutylpiperidine, and mibefradil, a tetralol derivative, all inhibited $Ca_v2.2$ calcium responses with potencies similar to EP literature values (Fig. 4, Table 1). Rank order of potency matched the literature as follows: ctx-GVIa > ctx-MVIIa ≫ cadmium > flunarizine > fluspirilene > mibefradil (Table 1). Linear regression analysis revealed a significant correlation between FLIPR IC_{50} values for each cell line versus EP literature values as cited in Table 1: $p < 0.001$ for $\alpha1_B$, $\alpha2\delta$, β_3-HEK IC_{50} versus EP IC_{50}; $p < 0.001$ for $\alpha1_B$, β_3-HEK IC_{50} versus EP IC_{50}.

Pharmacologically, many small molecules have been described with dual Na^+/Ca^{2+} channel-blocking activity [26,47–50]. This dual pharmacological activity has been proposed as important for the therapeutic efficacy of some compounds [34,38]. Thus, the pharmacologies of known Na^+ channel inhibitors of varying chemical classes were characterized in the $\alpha1_B$, $\alpha2\delta$, β_3-HEK and $\alpha1_B$, β_3-HEK cells. Compounds with Na^+ channel EP K_i values of <400 nM that exemplify three different structural chemotypes [51,52], a 3-(4-phenoxyphenyl) pyrazole (compound 18), a phenoxy phenylpyridine (compound 24), and an (aryloxy)aryl semicarbazone (PBSC) exhibited $Ca_v2.2$

Table 2 – $Ca_v2.2$ FLIPR IC_{50} vs. Na^+ channel EP K_i values for reference Na^+ channel inhibitors

Compound	N-VGCC FLIPR IC_{50} (μM)		Literature Na^+ channel EP	
	$\alpha1_B$, $\alpha2\delta$, β_3	$\alpha1_B$, β_3	K_i (μM)	Reference
Group 1. Diverse chemotypes				
Riluzole	0.27 ± 0.53 (3)	1.51 ± 0.42 (4)	0.20	[69]
GBR-12935	0.85 ± 0.51 (3)	0.97 ± 0.32 (3)	0.034	[70]
ST-148 maleate	2.36 ± 0.23 (3)	2.67 ± 0.78 (3)	0.57	[70]
RBI 257 maleate	0.99 ± 0.23 (3)	0.98 ± 0.21 (3)	0.64	[70]
Butaclamol	2.13 ± 0.21 (4)	1.74 ± 0.53 (4)	1.61	[70]
R59949	>20 (5)	>20 (4)	5.34[a]	[70]
PBSC	>20 (3)	>20 (6)	0.35	[51]
Group 2. Phenoxyphenyl pyridines				
12	2.29 ± 0.33 (4)	2.63 ± 0.60 (3)	0.028	[51]
6	0.89 ± 0.39 (3)	0.31 ± 0.13 (3)	0.096	
23	13.57 ± 4.74 (3)	18.70 ± 4.81 (4)	0.12	
18	4.70 ± 0.50 (3)	1.39 ± 0.62 (3)	0.15	
22c	6.70 ± 1.06 (3)	3.78 ± 1.65 (4)	0.18	
25	3.17 ± 1069 (3)	6.16 ± 2.49 (5)	0.26	
24	0.47 ± 0.21 (4)	1.12 ± 0.39 (4)	0.37	
22a	2.89 ± 0.50 (3)	1.77 ± 0.76 (5)	0.39	
15	7.87 ± 3.45 (4)	16.83 ± 6.18 (3)	0.60	
9	6.88 ± 0.88 (3)	21.49 ± 11.22 (5)	13.40	
Group 3. 3-(4-Phenoxyphenyl) pyrazoles				
19	3.83 ± 1.85 (4)	2.46 ± 0.86 (3)	0.025	[52]
15	2.24 ± 0.89 (4)	5.08 ± 3.52 (3)	0.031	
18	0.65 ± 0.24 (5)	0.098 ± 0.0443 (3)	0.031	
17	0.71 ± 0.26 (3)	1.27 ± 0.46 (4)	0.034	
14	3.83 ± 1.85 (4)	9.50 ± 3.21 (4)	0.035	
13	6.44 ± 0.70 (3)	10.27 ± 3.30 (4)	0.69	

Values represent mean ± S.E.M. (*n*). Na^+ channel EP K_i values are derived from the literature as referenced. PBSC refers to 4-(4-fluorophenoxy)benzaldehyde semicarbazone.

[a] Data value is from a non-EP assay of Na^+ channel function.

IC_{50} values ranging from 100 nM to >20 μM (Fig. 5). Testing of a larger set of Na^+ channel inhibitor compounds representing these and other chemical series revealed that average $Ca_v2.2$ IC_{50} values matched well between the two recombinant cell lines and correlated significantly (Fig. 6, Table 2). However, these values were generally inconsistent with published Na^+ channel EP K_i values, and did not correlate with Na^+ channel activity for either cell line (Fig. 6, Table 2). Nonetheless, a substantial proportion of the known Na^+ channel inhibitors tested did exhibit activity at $Ca_v2.2$ in these cells, thereby demonstrating a previously uncharacterized dual Na^+/Ca^{2+} inhibitor pharmacology for these compounds.

The class of compounds collectively described as antidepressants has been increasingly associated with secondary Na^+ [39,53–56] and/or Ca^{2+} [35–37,57,58] channel-blocking activity. These secondary biological activities have been proposed to underlie some additional therapeutic effects of these compounds as well as to be mechanistically involved in some clinically observed side effects. Thus, $Ca_v2.2$ pharmacology for antidepressants of different chemical classes and varying primary pharmacological activity was characterized (Fig. 7, Table 3). Most compounds showed some degree of blocking activity, though potencies were generally moderate-to-low. Average IC_{50} values matched well between the two recombinant cell lines (Table 3), thus demonstrating a previously uncharacterized secondary pharmacology at $Ca_v2.2$ for several of these compounds.

4. Discussion

$Ca_v2.2$ is a neuronal, presynaptically expressed, voltage-dependent calcium channel that functions to regulate neurotransmitter release [2–5]. It is a clinically validated target for the treatment of human chronic pain [8], has been implicated in mechanisms of neuronal excitotoxicity [7,59], and is involved in sympathetic nervous system regulation of cardiovascular tissue [2,9]. Pharmacologically, a variety of blocking agents of $Ca_v2.2$ have been described and extensively characterized [18–20,23–27]. However, a systematic, well-validated pharmacological analysis of this target that would make feasible the determination of relative compound potency, rank order, and structure–activity relationship is lacking. Thus, we have pharmacologically characterized $Ca_v2.2$ in two recombinant cell lines: $\alpha1_B$, $\alpha2\delta$, β_3-HEK-293 and $\alpha1_B$, β_3-HEK-293 using calcium mobilization. Validation of this approach with respect to reference antagonists from the literature was demonstrated. The pharmacology of $Ca_v2.2$ was then extended to novel classes of compounds represented by molecules previously characterized with other primary pharmacologies, namely Na^+ channel inhibitors and antidepressants.

The pharmacological approach chosen for these studies entailed calcium mobilization measurement of $Ca_v2.2$ function. Although not as information rich as EP with respect to determination of state-dependence and compound-channel

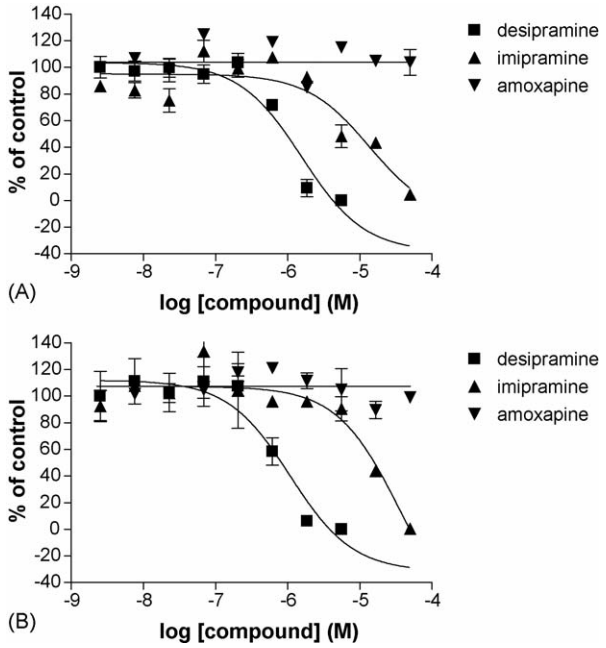

Fig. 7 – Concentration-dependent antidepressant compound inhibition of calcium responses measured on FLIPR^{96} in $\alpha1_B$, $\alpha2\delta$, β_3- and $\alpha1_B$, β_3-HEK-293 cells. (A) Desipramine, imipramine, and amoxapine mediated concentration-dependent inhibition of the calcium mobilization response to 90 mM KCl in $\alpha1_B$, $\alpha2\delta$, β_3-HEK-293 cells. Data points are the mean ± S.E.M. of four wells from one plate representative of 3–4. (B) Same compounds as panel A measured from $\alpha1_B$, β_3-HEK-293 cells. Data points are the mean ± S.E.M. of four wells from one plate representative of 3–4.

mechanism of interaction, this approach still delivers a functional read-out of channel activity with sufficient throughput to support pharmacological analysis such as rank order of potency and structure–activity relationship. Additionally this approach avoids the limitations of radiolabeled toxin binding techniques that are biased toward detection of compounds that directly or allosterically interfere with toxin binding [21,22]. A calcium mobilization approach to measuring $Ca_v2.2$ has been demonstrated previously [18,28–33]. However, we have extended the credibility of this strategy by conducting a comprehensive validation of our methods with respect to potency and rank order for multiple classical $Ca_v2.2$ reference inhibitors originally characterized by EP and which represent varying chemical classes and a large dynamic range of potency (~1–2000 nM). Interestingly, our methods require a 1 h compound pretreatment to achieve potency values comparable to EP. This parameter is optimal likely because it permits compounds to reach full equilibrium with respect to steady-state inactivation at all concentrations.

A current concept in the development of novel inhibitors of $Ca_v2.2$ is state-dependence [60,61]. Our data indicate that the present approach is sensitive to inhibition by small molecules that have been characterized as exhibiting voltage-dependent, frequency-dependent, and/or use-dependent mechanism of block. Specifically flunarizine, fluspirilene, and mibefradil have been demonstrated to mechanistically exhibit some or all of these properties [23,24,27]. In addition, cadmium has been described mechanistically as an open-channel blocker of calcium channels [62,63]. Our approach appropriately detects this type of pharmacological inhibitor as well. The conotoxins, which also inhibit in this assay, are generally regarded as state-independent, as they bind any state of the channel with equal affinity. Thus our data are insufficient to conclude whether or to what extent the method preferentially measures state-dependent block. Under our experimental conditions, the channels likely exist as a mixture of various gating states and thus the potency may reflect contributions of all gating categories.

A substantial number of molecules that have been described as Na^+ channel blockers have also been identified as calcium channel blockers [26,34,38,47–50]. Such compounds include 4-arylpiperidines and 4-aryl-4-piperidinols, an analogue of the anti-epileptic lamotrigine termed 619C89, a neuroprotectant known as riluzole, and the diphenylalkylpiperazines flunarizine and lidoflazine. This dual Na^+/Ca^{2+} channel pharmacological activity has been proposed as important for the therapeutic efficacy of some compounds [34,38]. Thus we extended the pharmacology of the recombinant $Ca_v2.2$ calcium mobilization response to an analysis of various known Na^+ channel inhibitors representing multiple chemotypes. Most compounds did indeed exhibit a secondary

Table 3 – FLIPR IC_{50} values at $Ca_v2.2$ for various antidepressant compounds

Antidepressant	FLIPR IC_{50} (μM)		Primary pharmacology
	$\alpha1_B$, $\alpha2\delta$, β_3	$\alpha1_B$, β_3	
Desipramine	0.41 ± 0.18 (4)	0.96 ± 0.18 (4)	NE/5-HT transporter inhibition
Amitriptyline	4.51 ± 0.77 (5)	7.51 ± 0.86 (4)	NE/5-HT transporter inhibition
Clomipramine	5.12 ± 0.83 (4)	1.96 ± 0.52 (3)	NE/5-HT transporter inhibition
Mianserin	5.23 ± 0.25 (3)	6.21 ± 0.55 (3)	5-HT2 antagonist/inverse agonist
Citalopram	8.58 ± 3.33 (4)	26.28 ± 2.92 (3)	5-HT uptake inhibition
Fluoxetine	10.16 ± 4.83 (6)	11.70 ± 1.26 (4)	5-HT uptake inhibition
Doxepin	10.38 ± 3.50 (3)	14.59 ± 4.94 (4)	NE/5-HT transporter inhibition
Buproprion	10.57 ± 4.14 (3)	23.21 ± 5.23 (3)	DA/NE uptake inhibition
Imipramine	15.81 ± 4.16 (4)	>20 (3)	NE/5-HT transporter inhibition
Amoxapine	>20 (3)	>20 (4)	NE uptake/5-HT_2 inhibition

Values represent mean ± S.E.M. (*n*).

pharmacology at $Ca_v2.2$, with varying potencies, thereby identifying novel chemotypes at $Ca_v2.2$. Rank order of potency did not match that of Na^+ channels across or within chemotypes, thereby indicating that the structure–activity relationship for $Ca_v2.2$ inhibition is different than that of Na^+ channel inhibition. However, given that the majority of these compounds demonstrated an additional $Ca_v2.2$ blocking activity, it may be warranted to consider $Ca_v2.2$ as a counter-screen in drug discovery programs aimed at targeting Na^+ channels, or vice versa, to monitor compound selectivity.

Similar to the Na^+ channel inhibitors, antidepressants as a class have been increasingly associated with secondary Ca^{2+} channel pharmacology that may contribute additional therapeutic effects or mechanistically underlie some clinically observed side effects [35–37,57,58]. Antidepressants with already described secondary Ca^{2+} channel pharmacology include fluoxetine, imipramine, and clomipramine. We have extended the $Ca_v2.2$ pharmacological characterization to additional tricyclics, selective serotonin reuptake inhibitors (SSRIs), and various other classes of antidepressants with previously uncharacterized $Ca_v2.2$ activity. Within the tricyclic category were included desipramine, amitriptyline, clomipramine, doxepin, imipramine, and amoxapine. These compounds exhibited a broad range of $Ca_v2.2$ potencies, with desipramine as the most potent and amoxapine the least. Clinically, desipramine has been reported to produce the greatest reduction in postherpetic neuralgia pain when compared to amitriptyline or fluoxetine [64]. Additionally, desipramine is a major active metabolite of imipramine and is the product of cytochrome P450 mediated N-demethylation of its parent compound [65]. Metabolic conversion of imipramine to a more potent $Ca_v2.2$ inhibitor could play a role in imipramine's observed efficacy in human neuropathic pain [66], as well as in its risk of orthostatic hypotension in patients with impaired left ventricular function [67]. Thus more detailed mechanistic investigation into desipramine's and imipramine's secondary pharmacology at $Ca_v2.2$ or other calcium channels, and the relationship to clinical effect is warranted. The SSRIs fluoxetine and citalopram exhibited moderate to low potency at $Ca_v2.2$, as did the tetracyclic antidepressant mianserin, and the newer generation modified antidepressant compound buproprion.

Electrophysiologically, the $\alpha1_B$, $\alpha2\delta$, β_3-HEK cells exhibited robust $Ca_v2.2$ currents ($\geq$0.5 nA) appropriately blocked by ctx-MVIIa and cadmium. However the $\alpha1_B$, β_3-HEK cell currents were dramatically smaller in amplitude ($\leq$200 pA) such that they were not feasible for systematic biophysical or pharmacological analyses. This is consistent with the well-characterized role of the $\alpha2\delta$ subunit in enhancement of calcium channel current amplitude [46] through regulation of $\alpha1$ subunit trafficking [46,68]. Interestingly, our data has shown that calcium mobilization responses are readily detectable in both cell lines, and can be utilized for systematic pharmacological analysis. As such, the overall pharmacological profiles matched closely between the triple subunit ($\alpha1_B$, $\alpha2\delta$, β_3) and dual subunit ($\alpha1_B$, β_3) cell lines across a multiplicity of chemotypes, a large dynamic range of compound potencies, and varying primary pharmacological classes. These data suggest that at a macroscopic level, the $\alpha2\delta$ subunit does not predominantly influence compound blockade of $Ca_v2.2$. It has been reported that in the presence of $\alpha2\delta$, $Ca_v2.2$ affinity measured by EP for ω-conotoxins is lower than in the absence of $\alpha2\delta$ [16]. This effect is more prominent for $Ca_v2.2$ expressed in *Xenopus* oocytes than in HEK-293 cells [16]. Our data, generated from $Ca_v2.2$ expressed in HEK-293 cells shows a similar trend, particularly for ctx-MVIIa, but is less pronounced than the previously reported oocyte data, and is qualitatively more comparable to such observations from HEK-293 cells [16].

In summary, this study has provided a more comprehensive pharmacological characterization of $Ca_v2.2$ inhibitors in two recombinant cell lines using a calcium mobilization approach. The approach was validated with respect to potency and rank order for multiple classical $Ca_v2.2$ reference inhibitors of various different chemical classes, and most interestingly for several voltage-dependent and/or open channel-blocking compounds. The pharmacology of $Ca_v2.2$ was then extended to novel chemotypes within the Na^+ channel inhibitor and antidepressant classes of compounds. The data revealed that compounds within these classes do inhibit $Ca_v2.2$ with varying potencies and that the pharmacological profiles at $Ca_v2.2$ correlate significantly between the two cell lines.

REFERENCES

[1] Catterall WA, Perez-Reyes E, Snutch TP, Striessnig J. International Union of Pharmacology. XLVIII. Nomenclature and structure–function relationships of voltage-gated calcium channels. Pharmacol Rev 2005;57:411–25.

[2] Hirning LD, Fox AP, McCleskey EW, Olivera BM, Thayer SA, Miller RJ, et al. Dominant role of N-type Ca^{2+} channels in evoked release of norepinephrine from sympathetic neurons. Science 1988;239:57–61.

[3] Luebke JI, Dunlap K, Turner TJ. Multiple calcium channel types control glutamatergic synaptic transmission in the hippocampus. Neuron 1993;11:895–902.

[4] Takahashi T, Momiyama A. Different types of calcium channels mediate central synaptic transmission. Nature 1993;366:156–8.

[5] Wheeler DB, Randall A, Tsien RW. Roles of N-type and Q-type Ca^{2+} channels in supporting hippocampal synaptic transmission. Science 1994;264:107–11.

[6] Altier C, Zamponi GW. Targeting Ca^{2+} channels to treat pain: T-type versus N-type. Trends Pharmacol Sci 2004;25:465–70.

[7] Perez-Pinzon MA, Yenari MA, Sun GH, Kunis DM, Steinberg GK. SNX-111. a novel, presynaptic N-type calcium channel antagonist, is neuroprotective against focal cerebral ischemia in rabbits. J Neurol Sci 1997;153: 25–31.

[8] Staats PS, Yearwood T, Charapata SG, Presley RW, Wallace MS, Byas-Smith M, et al. Intrathecal ziconotide in the treatment of refractory pain in patients with cancer or AIDS. JAMA 2004;291:63–70.

[9] Mori Y, Nishida M, Shimizu S, Ishii M, Yoshinaga T, Ino M, et al. Calcium channel alpha1B subunit ($Ca_v2.2$) knockout mouse reveals a predominant role of N-type channels in the sympathetic regulation of the circulatory system. Trends Cardiovasc Med 2002;12:270–5.

[10] McEnery MW, Snowman AM, Sharp AH, Adams ME, Snyder SH. Purified omega-conotoxin GVIA receptor of rat brain

resembles a dihydropyridine-sensitive L-type calcium channel. Proc Natl Acad Sci USA 1991;88:11095–9.
[11] Lin Z, Haus S, Edgerton J, Lipscombe D. Identification of functionally distinct isoforms of the N-type calcium channel in rat sympathetic ganglia and brain. Neuron 1997;18:153–66.
[12] Lin Z, Lin Y, Schorge S, Pan JQ, Beierlein M, Lipscombe D. Alternative splicing of a short cassette exon in alpha1B generates functionally distinct N-type calcium channels in central and peripheral neurons. J Neurosci 1999;19:5322–31.
[13] Pan JQ, Lipscombe D. Alternative splicing in the cytoplasmic II–III loop of the N-type Ca channel alpha 1B subunit: functional differences are beta subunit-specific. J Neurosci 2000;20:4769–75.
[14] Arikkath J, Campbell KP. Auxiliary subunits: essential components of the voltage-gated calcium channel complex. Curr Opin Neurobiol 2003;13:298–307.
[15] Stea A, Dubel SJ, Pragnell M, Leonard JP, Campbell KP, Snutch TP. A beta subunit normalizes the electrophysiological properties of a cloned N-type Ca^{2+} channel alpha1 subunit. Neuropharmacology 1993;32: 1103–16.
[16] Mould J, Yasuda T, Schroeder CI, Beedle AM, Doering CJ, Zamponi GW, et al. The alpha2delta auxiliary subunit reduces affinity of omega-conotoxins for recombinant N-type ($Ca_v2.2$) calcium channels. J Biol Chem 2004;279:34705–14.
[17] Gee NS, Brown JP, Dissanayake VU, Offord J, Thurlow R, Woodruff GN. The novel anticonvulsant drug, gabapentin (neurontin), binds to the alpha2delta subunit of a calcium channel. J Biol Chem 1996;271:5768–76.
[18] Bleakman D, Bowman D, Bath CP, Brust PF, Johnson EC, Deal CR, et al. Characteristics of a human N-type calcium channel expressed in HEK293 cells. Neuropharmacology 1995;34:753–65.
[19] Boland LM, Morrill JA, Bean BP. omega-Conotoxin block of N-type calcium channels in frog and rat sympathetic neurons. J Neurosci 1994;14:5011–27.
[20] Kaneko S, Cooper CB, Nishioka N, Yamasaki H, Suzuki A, Jarvis SE, et al. Identification and characterization of novel human $Ca_v2.2$ (alpha1B) calcium channel variants lacking the synaptic protein interaction site. J Neurosci 2002;22:82–92.
[21] Baell JB, Duggan PJ, Forsyth SA, Lewis RJ, Lok YP, Schroeder CI. Synthesis and biological evaluation of nonpeptide mimetics of omega-conotoxin GVIA. Bioorg Med Chem 2004;12:4025–37.
[22] Nielsen KJ, Schroeder T, Lewis R. Structure–activity relationships of omega-conotoxins at N-type voltage-sensitive calcium channels. J Mol Recogn 2000;13:55–70.
[23] Bezprozvanny I, Tsien RW. Voltage-dependent blockade of diverse types of voltage-gated Ca^{2+} channels expressed in *Xenopus* oocytes by the Ca^{2+} channel antagonist mibefradil (Ro 40-5967). Mol Pharmacol 1995;48:540–9.
[24] Sah DW, Bean BP. Inhibition of P-type and N-type calcium channels by dopamine receptor antagonists. Mol Pharmacol 1994;45:84–92.
[25] Spedding M, Kenny B, Chatelain P. New drug binding sites in calcium channels. Trends Pharmacol Sci 1995;16:139–42.
[26] Stefani A, Hainsworth AH, Spadoni F, Bernardi G. On the inhibition of voltage activated calcium currents in rat cortical neurones by the neuroprotective agent 619C89. Br J Pharmacol 1998;125:1058–64.
[27] Tytgat J, Pauwels PJ, Vereecke J, Carmeliet E. Flunarizine inhibits a high-threshold inactivating calcium channel (N-type) in isolated hippocampal neurons.. Brain Res 1991;549:112–7.
[28] Hu LY, Ryder TR, Rafferty MF, Taylor CP, Feng MR, Kuo BS, et al. The discovery of [1-(4-dimethylamino-benzyl)-piperidin-4-yl]-[4-(3,3-dimethylbutyl)-phenyl]-(3-methyl-but-2-enyl)-amine, an N-type Ca^{2+} channel blocker with oral activity for analgesia. Bioorg Med Chem 2000;8: 1203–12.
[29] Seko T, Kato M, Kohno H, Ono S, Hashimura K, Takenobu Y, et al. L-Cysteine based N-type calcium channel blockers: structure–activity relationships of the C-terminal lipophilic moiety, and oral analgesic efficacy in rat pain models. Bioorg Med Chem Lett 2002;12:2267–9.
[30] Seko T, Kato M, Kohno H, Ono S, Hashimura K, Takimizu H, et al. Structure–activity study and analgesic efficacy of amino acid derivatives as N-type calcium channel blockers. Bioorg Med Chem Lett 2001;11:2067–70.
[31] Seko T, Kato M, Kohno H, Ono S, Hashimura K, Takimizu H, et al. Structure–activity study of L-cysteine-based N-type calcium channel blockers: optimization of N- and C-terminal substituents. Bioorg Med Chem Lett 2002;12:915–8.
[32] Seko T, Kato M, Kohno H, Ono S, Hashimura K, Takimizu H, et al. Structure–activity study of L-amino acid-based N-type calcium channel blockers. Bioorg Med Chem 2003;11: 1901–13.
[33] Teodori E, Baldi E, Dei S, Gualtieri F, Romanelli MN, Scapecchi S, et al. Design, synthesis, and preliminary pharmacological evaluation of 4-aminopiperidine derivatives as N-type calcium channel blockers active on pain and neuropathic pain. J Med Chem 2004;47:6070–81.
[34] Aoki Y, Tamura M, Itoh Y, Ukai Y. Cerebroprotective action of a Na^+/Ca^{2+} channel blocker NA-7 I. Effect on the cerebral infarction and edema at the acute stage of permanent middle cerebral artery occlusion in rats. Brain Res 2001;890:162–9.
[35] Becker B, Morel N, Vanbellinghen AM, Lebrun P. Blockade of calcium entry in smooth muscle cells by the antidepressant imipramine. Biochem Pharmacol 2004;68:833–42.
[36] Deak F, Lastoczi B, Pacher P, Petheo GL, Kecskemeti V, Spat A. Inhibition of voltage-gated calcium channels by fluoxetine in rat hippocampal pyramidal cells. Neuropharmacology 2000;39:1029–36.
[37] Magyar J, Rusznak Z, Harasztosi C, Kortvely A, Pacher P, Banyasz T, et al. Differential effects of fluoxetine enantiomers in mammalian neural and cardiac tissues. Int J Mol Med 2003;11:535–42.
[38] O'Neill MJ, Bath CP, Dell CP, Hicks CA, Gilmore J, Ambler SJ, et al. Effects of Ca^{2+} and Na^+ channel inhibitors in vitro and in global cerebral ischemia in vivo. Eur J Pharmacol 1997;332:121–31.
[39] Benjamin ER, Olanrewaju S, Pruthi F, Lavery D, Ilyin VI, Valenzano KJ. Pharmacological characterization of recombinant N-type calcium channel mediated calcium mobilization using FLIPR. Abstract Viewer/itinerary Planner Washington, DC: Society for Neuroscience, 2005. Online 2005; Program No. 265.9.
[40] Castellano A, Wei X, Birnbaumer L, Perez-Reyes E. Cloning and expression of a neuronal calcium channel beta subunit. J Biol Chem 1993;268:12359–66.
[41] Dubel SJ, Starr TV, Hell J, Ahlijanian MK, Enyeart JJ, Catterall WA, et al. Molecular cloning of the alpha-1 subunit of omega-conotoxin sensitive calcium channel. Proc Natl Acad Sci USA 1992;89:5058–62.
[42] Kim HL, Kim H, Lee P, King RG, Chin H. Rat brain expresses an alternatively spliced form of the dihydropyridine-sensitive L-type calcium channel alpha2 subunit. Proc Natl Acad Sci USA 1992;89:3251–5.
[43] Hamill OP, Marty A, Neher E, Sakmann B, Sigworth FJ. Improved patch-clamp techniques for high-resolution current recording from cells and cell-free membrane patches. Pflugers Arch 1981;391:85–100.
[44] Bean BP. Classes of calcium channels in vertebrate cells. Annu Rev Physiol 1989;51:367–84.

[45] Wakamori M, Strobeck M, Niidome T, Teramoto T, Imoto K, Mori Y. Functional characterization of ion permeation pathway in the N-type calcium channel. J Neurophysiol 1998;79:622–34.
[46] Singer D, Biel M, Lotan I, Flockerzi V, Hofmann F, Dascal N. The roles of the subunits in the function of the calcium channel. Science 1991;253:1553–7.
[47] Annoura H, Nakanishi K, Uesugi M, Fukunaga A, Imajo S, Miyajima A, et al. Synthesis and biological evaluation of new 4-arylpiperidines and 4-aryl-4-piperidinols: dual Na^+ and Ca^{2+} channel blockers with reduced affinity for dopamine D2 receptors. Biorg Med Chem 2002;10:371–83.
[48] Annoura H, Nakanishi K, Uesugi M, Fukunaga A, Miyajima A, Tamura-Horikawa Y, et al. A novel class of Na^+ and Ca^{2+} channel dual blockers with highly potent anti-ischemic effects. Bioorg Med Chem Lett 1999;9:2999–3002.
[49] Geer JJ, Dooley DJ, Adams ME. K^+ stimulated $^{45}Ca^{2+}$ flux into rat neocortical mini-slices is blocked by omega-Aga-IVA and the dual Na^+/Ca^{2+} channel blockers lidoflazine and flunarizine. Neurosci Lett 1993;158:97–100.
[50] Stefani A, Spadoni F, Bernardi G. Differential inhibition by riluzole, lamotrigine and phenytoin of sodium and calcium currents in cortical neurons, implications for neuroprotective strategies. Exp Neurol 1997;147:115–22.
[51] Shao B, Victory S, Ilyin VI, Goehring RR, Sun Q, Hogenkamp D, et al. Phenoxyphenyl pyridines as novel state-dependent, high-potency sodium channel inhibitors. J Med Chem 2004;47:4277–85.
[52] Yang J, Gharagozloo P, Yao J, Ilyin VI, Carter RB, Nguyen P, et al. 3-(4-Phenoxyphenyl)pyrazoles: a novel class of sodium channel blockers. J Med Chem 2004;47:1547–52.
[53] Barber MJ, Starmer CF, Grant AO. Blockade of cardiac sodium channels by amitriptyline and diphenylhydantoin. Evidence for two use-dependent binding sites. Circ Res 1991;69:208–14.
[54] Nau C, Seaver M, Wang SY, Wang GK. Block of human heart hH1 sodium channels by amitriptyline. J Pharmacol Exp Ther 2000;292:1015–23.
[55] Pancrazio JJ, Kamatchi GL, Roscoe AK, Lynch C. Inhibition of neuronal Na^+ channels by antidepressant drugs. J Pharmacol Exp Ther 1998;284:208–14.
[56] Yang YC, Kuo CC. Inhibition of Na^+ current by imipramine and related compounds: different binding kinetics as an inactivation stabilizer and as an open channel blocker. Mol Pharmacol 2002;62:1228–37.
[57] Mousavizadeh K, Ghafourifar P, Sadeghi-Nejad H. Calcium channel blocking activity of thioridazine, clomipramine and fluoxetine in isolated rat vas deferens: a relative potency measurement study. J Urol 2002;168:2716–9.
[58] Wang SJ, Su CF, Kuo YH. Fluoxetine depresses glutamate exocytosis in the rat cerebrocortical nerve terminals (synaptosomes) via inhibition of P/Q-type Ca^{2+} channels. Synapse 2003;48:170–7.
[59] Kimura M, Sawada K, Miyagawa T, Kuwada M, Katayama K, Nishizawa Y. Role of glutamate receptors and voltage-dependent calcium and sodium channels in the extracellular glutamate/aspartate accumulation and subsequent neuronal injury induced by oxygen/glucose deprivation in cultured hippocampal neurons. J Pharmacol Exp Ther 1998;285:178–85.
[60] Hille B. Local anesthetics: hydrophilic and hydrophobic pathways for the drug–receptor reaction. J Gen Physiol 1977;69:497–515.
[61] Winquist RJ, Pan JQ, Gribkoff VK. Use-dependent blockade of $Ca_v2.2$ voltage-gated calcium channels for neuropathic pain. Biochem Pharmacol 2005;70:489–99.
[62] Chow RH. Cadmium block of squid calcium currents. Macroscopic data and a kinetic model. J Gen Physiol 1991;98:751–70.
[63] Vennekens R, Prenen J, Hoenderop JG, Bindels RJ, Droogmans G, Nilius B. Pore properties and ionic block of the rabbit epithelial calcium channel expressed in HEK 293 cells. J Physiol 2001;530:183–91.
[64] Rowbotham MC, Reisner LA, Davies PS, Fields HL. Treatment response in antidepressant-naive postherpetic neuralgia patients: double-blind, randomized trial. J Pain 2005;6:741–6.
[65] Lemoine A, Gautier JC, Azoulay D, Kiffel L, Belloc C, Guengerich FP, et al. Major pathway of imipramine metabolism is catalyzed by cytochromes P-450 1A2 and P-450 3A4 in human liver. Mol Pharmacol 1993;43:827–32.
[66] Rasmussen PV, Jensen TS, Sindrup SH, Bach FW. TDM-based imipramine treatment in neuropathic pain. Ther Drug Monit 2004;26:352–60.
[67] Glassman AH. Cardiovascular effects of tricyclic antidepressants. Annu Rev Med 1984;35:503–11.
[68] Canti C, Nieto-Rostro M, Foucault I, Heblich F, Wratten J, Richards MW, et al. The metal-ion-dependent adhesion site in the Von Willebrand factor-A domain of alpha2delta subunits is key to trafficking voltage-gated calcium channels. Proc Natl Acad Sci USA 2005;102:11230–5.
[69] Hebert T, Drapeau P, Pradier L, Dunn RJ. Block of the rat brain IIA sodium channel alpha subunit by the neuroprotective drug riluzole. Mol Pharmacol 1994;45:1055–60.
[70] Benjamin ER, Pruthi F, Olanrewaju S, Ilyin VI, Crumley G, Kutlina E, et al. State-dependent compound inhibition of $Na_v1.2$ sodium channels using the FLIPR V_m dye: on-target and off-target effects of diverse pharmacological agents. J Biomol Screen 2006;11:29–39.